Conclusions

The nose vortex observed by Werle and Hsieh is explained on the basis of separation patterns previously discussed by Wang. It is counterclockwise rather than clockwise, as implied in Werle's original sketch. It occurs only during the transition from an open separation to a completely closed separation over an inclined body. Because it occurs only under this limited circumstance, such vortex formation easily can go unnoticed, unless one searches for it. Calculation of such a nose vortex appears to require a complete Navier-Stokes approach, and is a task for the future. Note added during proof: Werle has just sent us two surface-flow pictures for a nearly-flat blunt-nosed cylinder at $\alpha = 10°$ and 15° which also indicates a vortex pattern similar to those in Figs. 2a and b.

References

[1]Werle, H., "Separation on Axisymmetrical Bodies at Low Speed," *La Recherche Aeronautique,* No. 90, Sept.-Oct. 1962 pp. 3-14.

[2]Stetson, K.F., "Boundary-Layer Separation on Slender Cones at Angle of Attack," *AIAA Journal,* Vol. 10, May 1972,pp. 642-648.

[3]Zakkay, V., Miyazawa, M., and Wang, C.R., "Lee Surface Flow Phenomena Over Space Shuttle at Large Angles of Attack at $M_\infty = 6$," CR-13250l, 1974, NASA; also AIAA paper 75-148, Jan. 1975.

[4]Hsieh, T., "An Investigation of Separated Flow about a Hemisphere-Cylinder at Zero to 19 deg. Incidences in the Mach Number Range form 0.6 to 1.5," to be published as AECD-TR.

[5]Wang, K.C., "Separation Patterns of Boundary Layer over an inclined Body of Revolution," *AIAA Journal.* Vol. 10, Aug. 1972, pp. 1044-1050.

[6]Wang, K.C., "Boundary Layer over a Blunt Body at High Incidence with an Open-Type of Separation," Proceedings of the Royal Society of London, Series A., Vol., 340, 1974, pp. 33-55.

[7]Geissler, W., "Three-Dimensional Laminar Boundary Layer over a Body of Revolution at Incidence and with Separation;" *AIAA Journal,* Vol. 12, Dec. 1974, pp. 1743-1745.

Approximate Statistics of Random Vector Magnitudes

Hamilton Hagar Jr.*
Jet Propulsion Laboratory, Pasadena, Calif.

Introduction

IT often is desirable to know, at least approximately, the mean and 99% value of the magnitude of a random vector with independent components. A related case, for example, is the computation of the corrective velocity 99% statistics in interplanetary spacecraft maneuver analyses. In general, let the random vector be denoted as

$$\bar{v} = \begin{bmatrix} x \\ y \\ z \end{bmatrix} \tag{1}$$

with magnitude $v \equiv |\bar{v}| = (x^2+y^2+z^2)^{1/2}$. If x, y, z are distributed normally, if $E(x) = E(y) = E(z) = 0$, and if $E(x^2) = E(y^2) = E(z^2) = \sigma^2$, then v is distributed Maxwellian with mean $(8/\pi\sigma)^{1/2}$ and variance $(3-8/\pi)\sigma^2$. If the vector is a two-vector, say, $z \equiv 0$ in v, then the distribution of v is Rayleigh, with mean $(\pi/2)^{1/2}\sigma$ and variance $(2-\pi/2)\sigma^2$. A half-normal distribution results for $v = |x|$, with mean $(2/\pi)^{1/2}\sigma$ and variance $(1-2/\pi)\sigma^2$. These are special cases of χ distributions with degrees of freedom of 3, 2, 1, respectively (see, e.g., Refs. 1 and 2). The 99% values can be obtained directly from tables (e.g., Ref. 3) and for these cases are $v_{99} = 3.368\sigma$, $v_{99} = 3.035\sigma$, and $v_{99} = 2.576\sigma$, respectively.

The preceding, however, are very special cases, not applicable, in general, where the variances of x, y, and z are unequal. Although the case where $E(x^2) = E(y^2) = \sigma^2$, $E(z^2) = s^2$ is known,[4] and the general case for $E(x^2) = \sigma^2$, $E(y^2) = r^2$, and $E(z^2) = s^2$ has been solved,[5,6] generally these are computationally demanding. The next section presents simple, rough approximations for the mean and 99% values for random vectors of up to three independent elements.

Note that, when the elements of $\bar{v}$ are correlated, the problem may be reduced to the independent case by an appropriate transformation, $\bar{w} \equiv R\bar{v}$, so that

$$E(\bar{w}\bar{w}^T) = RE(\bar{v}\bar{v}^T)R^T = RVR^T = W \tag{2}$$

W is a diagonal matrix whose elements are the eigenvalues (all real) of the covariance matrix V; the columns of R are the corresponding eigenvectors. Because V is symmetric, $R^T = R^{-1}$; hence,

$$w = (\bar{w}^T\bar{w})^{1/2} = (\bar{v}^T R^T R\bar{v})^{1/2} = (\bar{v}^T\bar{v})^{1/2} = v \tag{3}$$

Development

A workable approach to approximating the mean and 99% values where x, y, and z have unequal variances can be obtained as functions of the means and 99% values for the respective individual cases with equal variances. Three forms for the approximation of both are

$$\alpha = \{c_1\sigma^2 + (c_2-c_1)(r^2+s^2)[(c_3-c_2)-(c_2-c_1)]rs\}^{1/2} \tag{4}$$

$$\beta = [c_1\sigma^2 + (c_2-c_1)r^2 + (c_3-c_2)s^2]^{1/2} \tag{5}$$

$$\gamma = (c_1)^{1/2}\sigma + [(c_2)^{1/2}-(c_1)^{1/2}]r + [(c_3)^{1/2}-(c_2)^{1/2}]s \tag{6}$$

where α, β, and γ represent either the mean or 99% value, $\sigma^2 = E(x^2)$, $r^2 = E(y^2)$, $s^2 = E(z^2)$, and c_1, c_2, and c_3 are coefficients associated with the one-, two-, and three- element vectors. These coefficients are presented in Table 1. They are the squares of the mean values and 99% values given in the Introduction. Thus, for the cases where 1) $\sigma = r = s$, 2) $\sigma = r$,

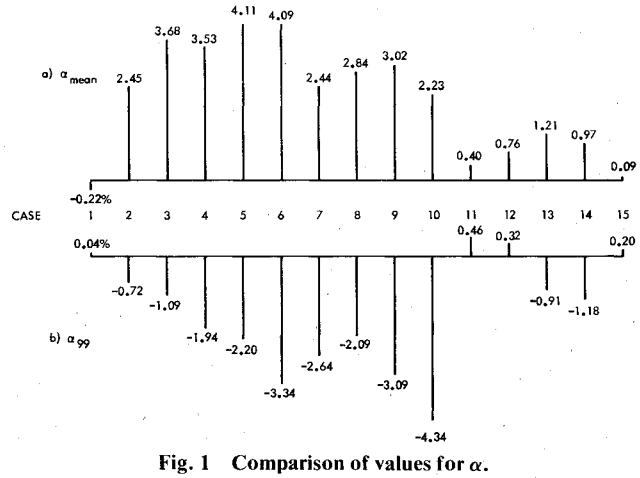

Fig. 1 Comparison of values for α.

Received Sept. 29, 1975; revision received March 5, 1976. This paper presents the results of one phase of research carried out at the Jet Propulsion Laboratory, California Institute of Technology, under Contract NAS7-100, sponsored by NASA.

Index categories: Aerospace Technology Utilization; Navigation, Control, and Guidance Theory; Spacecraft Mission Studies and Economics.

*Member of the Technical Staff. Member AIAA.

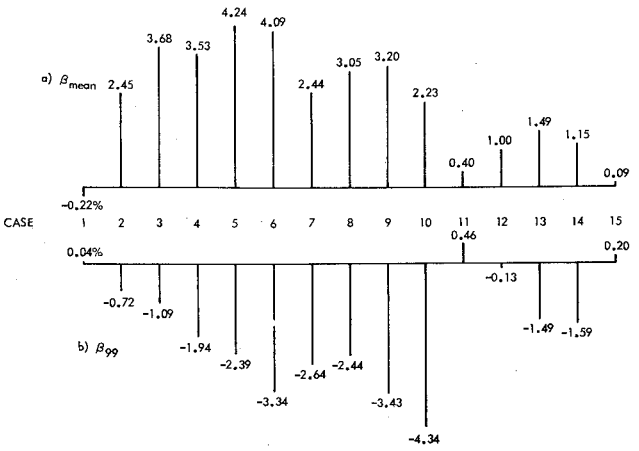

Fig. 2 Comparison of values for β.

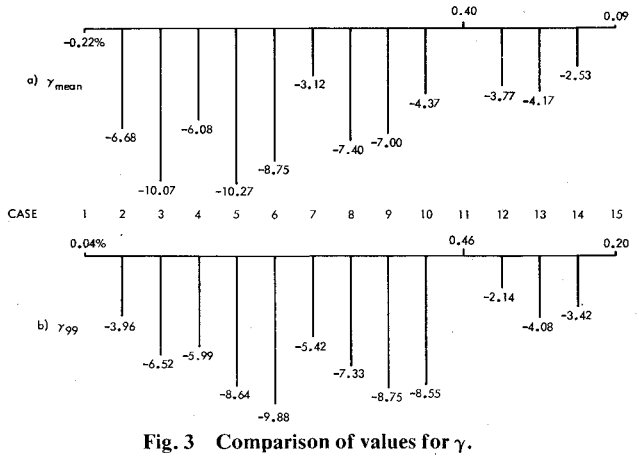

Fig. 3 Comparison of values for γ.

$s=0$; and 3) $r=s=0$, the equations reduce to their true mean and 99% values (the cases for the Maxwell, Rayleigh, and half-normal distributions).

When the coefficient values are substituted into Eq. (4), the results are

$$\alpha_{mean}=\left\{\frac{2}{\pi}\sigma^2+\left(\frac{\pi}{2}-\frac{2}{\pi}\right)\left(r^2+s^2\right)+\left(\frac{10}{\pi}-\pi\right)rs\right\}^{1/2} \tag{7}$$

$$\alpha_{99}=\left\{6.635^2+2.575\left(r^2+s^2\right)-0.444rs\right\}^{1/2} \tag{8}$$

with similar results for Eqs. (5) and (6). It should be noted that the best results have been obtained when σ is assigned the largest of the candidate values for (σ, r, s).

Numerical Results

To test the accuracy of each of the preceding approximating forms, Monte Carlo simulations were run for 15 different combinations of σ, r, and s. These values are given in Table 2 and are normalized so that $1\geq\sigma\geq r\geq s\geq 0$. The simulations were performed by generating pseudorandom values of $v=(x^2+y^2+z^2)^{1/2}$. The values were formed by obtaining pseudorandom samples of x, y, and z from an approximate, zero-mean gaussian distribution. The pseudorandom numbers were generated using Bell's algorithm, a modification of Box and Muller. The implementation is on the UNIVAC 1108 at the California Institute of Technology's Jet Propulsion Laboratory.

Table 1 Coefficients

α	c_1	c_2	c_3
Mean	$2/\pi$	$\pi/2$	$8/\pi$
v_{99}	6.635	9.210	11.341

Table 2 Simulation data

Case	σ	r	s
1	1	0	0
2	1	0.25	0
3	1	0.25	0.25
4	1	0.5	0
5	1	0.5	0.25
6	1	0.5	0.5
7	1	0.75	0
8	1	0.75	0.25
9	1	0.75	0.5
10	1	0.75	0.75
11	1	1	0
12	1	1	0.25
13	1	1	0.5
14	1	1	0.75
15	1	1	1

For each case, 10,000 samples each of x, y, and z were generated, and the mean and 99% values of $v=(x^2+y^2+z^2)^{1/2}$ were obtained. These were compared with the values computed by Eqs. (4-6) and the percent of error

$$P=(v_{\text{Monte Carlo}}-v_{\text{approx}})/v_{\text{Monte Carlo}}$$

given in Figs. 1-3 for α,β, and γ, respectively.

Note that, for cases 1, 11, and 15, the errors shown in each figure correspond to the errors from the true values, since all of the approximation equations are exact for these situations. Thus, these errors are due to the random number generation and are well under 1%.

For the α_{mean} and β_{mean}, the approximations for all but case 1 are overoptimistic, as shown by a positive percent of error. For all but one case, approximation of the 99% value for both the α and β forms yields a conservative value, as indicated by a negative percent of error. The exception is case 12 for α. Although the α form appears to yield slightly better results than β, for each of the cases investigated, the α and β approximations are all well within 5% of the Monte Carlo values.

The approximating form γ does not perform very well compared to α and β. Errors range to over 10% for γ_{mean} and over 9% for γ_{99}. Thus, of the forms and cases investigated, α appears to be the best.

An approximation to the second moment $E(v^2)$ also is available as the square of Eq. (7). It is suggested that the variance in v also may be approximated by Eq. (4), where

$$c_1=[1-(2/\pi)],\quad c_2=[2-(\pi/2)],\quad c_3=[3-(8/\pi)]\,.$$

are the coefficients of σ^2 for the half-normal, Rayleigh, and Maxwellian distributions, respectively. However, no substantiating numerical results have been obtained.

References

[1] Gray, H. L. and Odell, P. L., *Probability for Practicing Engineers*, Barnes & Nobel, Inc., New York, 1970, pp. 103-106.

[2] Papoulis, A., *Probability, Random Variables, and Stochastic Processes*, McGraw-Hill, New York, 1965, pp. 147-149, 250.

[3] Korn, G. A. and Korn, T. M., *Mathematical Handbook for Scientists and Engineers*, McGraw-Hill, New York, 1968, p. 1065.

[4] Beckman, P., *Scattering of Electromagnetic Waves from Rough Surfaces*, Pergamon, New York, 1963.

[5]Lee, B. G. and Boain, R. J., "Propellant Requirements for Mid-Course Velocity Corrections," *Journal of Spacecraft and Rockets*, Vol. 10, Dec. 1973, pp. 779-782.

[6]Lass, H., "Analysis of Random Speed in Midcourse Guidance," TM 391-374, Oct. 12, 1972, Jet Propulsion Lab., Pasadena, Calif. (internal document).

Navier-Stokes Solutions for Chemical Laser Flows: Cold Flows

Ajay P. Kothari* and John D. Anderson Jr.†
University of Maryland, College Park, Md.

COMPUTATIONAL fluid dynamics is growing rapidly as a new third dimension in aerodynamics, complementing both laboratory experiment and pure analysis.[1,2] Work is advancing on both numerical methods and applications to practical engineering problems. The present paper straddles both categories. In particular, the present authors have been developing finite-difference solutions for the Navier-Stokes equations applied to the chemically reacting viscous flow in chemical lasers.[3] In the process of calculating such flows, several different finite-difference techniques for solving the Navier-Stokes equations have been examined and tested. The purpose of this paper is to describe some numerical experiments dealing with these techniques; these results have impact on the numerical solution of the Navier-Stokes equations in general.

The physical problem is illustrated in Fig. 1. A stream of partially dissociated fluorine is mixed tangentially with a stream of H_2; both streams are diluted with He. Characteristic of many chemical lasers, the Reynolds number is assumed low enough that laminar flow prevails in the mixing region. The ensuing chemically reacting flow downstream of the nozzles in a chemical laser is described precisely by the complete, two-dimensional Navier-Stokes equations including multicomponent diffusion and finite-rate chemical reactions. However, for the present numerical experiments, the chemical kinetics have been "switched off" artificially in order to examine the purely fluid-dynamic behavior of the solution. Thus, the following results do not contain the influence of chemical reactions. Such "coldflows" are purely artificial because in nature H_2 and F_2 are hypergolic. However, such results are quite appropriate for the present investigation.

These equations, without the chemical production terms, can be cast into the form

$$\partial U/\partial t = -(\partial F/\partial x) - (\partial G/\partial y) \tag{1}$$

where U, F, and G are one-dimensional vectors. The vector U contains elements such as ρ, ρu, ρv, ρE *and* ρ_i (standard nomenclature), and F and G contain these, as well as the viscous terms involving x and y derivatives of u, v, T and ρ_i. The full equations are given in detail in Ref. 3.

The finite-difference schemes used to solve these equations are of the predictor-corrector type patterned after the thoughts of MacCormack.[4] A time-dependent solution is used to calculate the complete flowfield in steps of time, starting from arbitrarily assumed initial conditions and eventually approaching the steady-state flow at large values of time. This steady state is the desired result, and the time-dependent solution is simply a means to that end. The predictor-corrector procedure is to obtain the flowfield at time $(n+1)$ from

$$U_{n+1} = U_n + (\partial U/\partial t)_{av} \Delta t \tag{2}$$

where $(\partial U/\partial t)_{av}$ is an average of the values obtained from Eq. (1) evaluated first from the known flow at time n (the predictor), and then from the predicted flow at time $n+1$ (the corrector). The flow conditions at the nozzle exits ($x=0$ in Fig. 1) are specified and held fixed, invariant with time. The use of time-dependent solutions for chemically reacting flows is well documented, e.g., Refs. 5 and 6.

In Eq. (1), the spatial derivatives $\partial F/\partial x$, $\partial G/\partial y$, and the x and y derivatives of u, v, T, etc., are obtained from finite differences. Herein lies the essence of the four different techniques examined in the present paper as follows:

1) Central differences: central differencing for F, G, ρ, T, u, v, and ρ_i everywhere, at all times.

2) Partial MacCormack: forward and backward differencing for F, G for predictor-corrector steps, respectively, while using central differencing for ρ, T, u, v, and ρ_i.

3) Full MacCormack: predictor step-forward for F, G, and forward for ρ, T, u, v, ρ_i; corrector step-backward for F, G, and backward for ρ, T, u, v, ρ_i.

4) Modified MacCormack: predictor step-forward for F, G, and backward for $\rho, T u, v, \rho_i$; corrector step-backward for F, G, and forward for ρ, T, u, v, ρ_i.

The use of these four schemes for the spatial differencing leads to some striking comparsions in the numerical flowfield results, as described below. Consider again the physical picture in Fig. 1. Imagine a fixed point in the flowfield at $x/h=10$ and $y/h=0.5$. The temporal behavior of the pressure at this point is shown in Fig. 2, as calculated from the four schemes. Note that schemes 2 and 4 yield the proper asymptotic approach to a steady flow at large times, whereas scheme 1 is oscillatory. For this particular problem, scheme 3 was observed to be unstable, as also shown in Fig. 2.

Consider now the final steady-state flowfield at $x/h=10$. Figures 3-5 illustrate the velocity, F_2 density, and pressure profiles, respectively, across the flowfield, as calculated from the different schemes. Note that the use of central differences leads to wiggles in the profiles, whereas the modified MacCormack approach (scheme 4) yields perfectly smooth profiles. The wiggles introduced by central differences are evident particularly in the pressure profile shown in Fig. 5. These results clearly demonstrate the superiority of the modified MacCormack approach. This superiority is substantiated further by Griffin,[7] who has obtained identical comparisons for a completely different application , namely, the solution of the Navier-Stokes equations for the flow inside an internal combustion reciprocating engine. Moreover, the experience of the present authors is in line with suggestions from Hankey,[8] obtained after the present work was finished. For further details, see Ref. 3.

A comment is made on the boundary conditions at $y=0$ and $y=h$. Symmetry conditions hold at these boundaries, as can be seen from Fig. 1, which models a segment of the multinozzle flow characteristic of many chemical lasers; i.e., $\partial u/\partial y = \partial p/\partial y = \partial \rho_i/\partial y = v = 0$ at $y=0$ and $y=h$. In the present finite-difference scheme, the reflection principle[1] is used which is an accurate representation of boundary conditions on a line of symmetry; i.e., $P_{j+1}=P_{j-1}, T_{j+1} T_{j-1}, v_{j+1} = -v_{j-1}$, etc., where j is an index in the y direction, and j lies on the boundary itself. Examining the results in Figs. 3-5, straight lines are drawn between each grid point. For this reason, the gradients shown at the boundary are deceptive and

Received Jan. 12, 1976: revision received Feb. 26, 1976. This work was supported under AFOSR Grant No. 74-2575, with Lloyd R. Lawrence as Project Manager. Computer time was provided in part through the facilities of the Compter Science Center of the University of Maryland.

Index categories: Lasers; Viscous Nonboundary-Layer Flows.

*Graduate Research Assistant, Department of Aerospace Engineering.

†Professor and Chairman, Department of Aerospace Engineering. Associate Fellow AIAA.